Biomedicine & Healthcare Research

*Biomedicine & Healthcare Research 2026 July;7:42-50*

https://doi.org/10.71599/bhr.v7i1.182

Open Access

Original article

# The Role of Multiparametric Magnetic Resonance Imaging (MRI) (DWI and DCE-MRI) in Differentiating Parotid Tumors: A Retrospective Study of 42 Cases

**Malika El Omri, Islem Dakhli, Mouna Bellakhdher, Nawress Thabet, Wassim Kermani**

*Department of Ear, Nose, Throat and Head and Neck Surgery, Farhat Hached University Hospital, Sousse, Tunisia.*

**Abstract**

**Background**: Tumors of the parotid gland are complex. The surgical approach depends on the histology, location, and size of the tumor. Magnetic resonance imaging (MRI) is an important tool for accurate preoperative assessment of topography and infiltration; however, its role in pathological differentiation remains controversial.

**Purpose**: Our study aims to illustrate the results of MRI in parotid tumors and correlate them with histopathological findings.

**Materials and Methods:** A retrospective and analytical study was conducted on 42 patients with clinically suspected parotid tumors, collected over 12 years from 2011 to 2023. All patients underwent a multiparametric MRI protocol, including conventional sequences, diffusion-weighted imaging (DWI) with apparent diffusion coefficient (ADC) measurement, and dynamic contrast-enhanced (DCE-MRI) sequences. MRI results were then correlated with the definitive histopathological findings obtained after surgery. Statistical analysis was performed using SPSS software. The concordance between MRI and histology was assessed using the kappa coefficient.

**Results**: Histopathology revealed 31 benign tumors (73.8%), 5 malignant tumors (11.9%), and 6 pseudotumors (14.2%). For distinguishing benign from malignant tumors, MRI showed moderate agreement with histology (kappa = 0.58). However, excellent concordance was observed for specific diagnoses: pleomorphic adenoma (kappa = 0.85) and Warthin tumor (kappa = 0.91). Mean ADC values were significantly lower in malignant tumors compared to benign tumors ($p < 0.05$). Pleomorphic adenoma typically demonstrated a Type A dynamic enhancement curve, Warthin tumor a Type B curve, and mucoepidermoid carcinoma a Type C curve.

**Conclusion**: Multiparametric MRI with gadolinium enhancement and ADC assessment demonstrates high diagnostic accuracy for specific benign parotid tumors, particularly pleomorphic adenoma and Warthin tumor, despite a moderate overall performance in distinguishing benign from malignant lesions. These findings can guide surgeons in preoperative planning when specific benign entities are suspected.

***Keywords:*** Parotid gland, MRI, Pleomorphic adenoma, Warthin tumor, ADC

***Received: December 28, 2025; Accepted: April 26, 2026***

## 1. Introduction

Salivary gland tumors are rare, accounting for approximately 2 to 6.5% of all head and neck neoplasms and 0.5% of all malignant tumors [1,2]. The parotid gland is the most common site, representing nearly 70% of all salivary gland tumors, of which approximately 80% are benign [3,4]. Among benign tumors, pleomorphic adenoma is the most frequent (approximately 65%), followed by Warthin tumor (15 to 20%). Malignant tumors are less common, with mucoepidermoid carcinoma being the most prevalent, accounting for 10% of all salivary gland tumors and 30% of malignant salivary neoplasms [1,5].

A reliable distinction between benign and malignant parotid masses is crucial. However, clinical examination alone is often insufficient for this differentiation. Clinical signs remain nonspecific in the diagnosis of malignant parotid tumors. The presence of facial paralysis may suggest malignancy.

In addition, most parotid tumors, whether benign or malignant, tend to grow slowly, which further limits the diagnostic value of clinical assessment alone [1].

Surgical treatment is the main therapeutic approach, using techniques such as extracapsular dissection, partial parotidectomy, or radical parotidectomy with sacrifice of the facial nerve for malignant parotid tumors [2].

The diagnostic strategy is multimodal. Given that 80 to 90% of parotid tumors are located in the superficial lobe, ultrasound is generally the first-line imaging test for their diagnosis [2]. However, fine needle aspiration cytology (FNAC) is not always conclusive, due to difficulties in sampling and the high heterogeneity of parotid tumors [3].

According to some studies, FNAC detects malignancy in 72% to 84% of tumors [6]. Computed tomography (CT) scan allows for preoperative staging, but its role in characterizing parotid tumors remains limited [3].

Conventional MRI is widely used to evaluate various pathologies of the parotid gland, highlighting their morphological characteristics. Certain MRI signs, such as T2 hypointense signals, poorly defined contours, diffuse growth, infiltration of subcutaneous tissue, and the presence of lymphadenopathy, are indicative of parotid malignancy [6]. However, conventional MRI relies primarily on morphological features, which can be misleading.

Corresponding Author: Malika El Omri, Omri.malika6@gmail.com

Significant overlap exists between benign and malignant tumors in terms of signal intensity, margins, and enhancement patterns, particularly for low-grade malignancies that may mimic benign lesions [7]. This morphological overlap limits the diagnostic confidence of conventional MRI alone.

Advanced functional MRI techniques help overcome the limitations of conventional imaging by providing additional biological insight into tumor behavior. DWI with ADC allows assessment of tissue cellularity and cell membrane integrity. Malignant tumors, because of their high cellular density, tend to restrict the movement of water molecules and therefore demonstrate lower ADC values. In contrast, benign lesions generally exhibit higher ADC values, reflecting a more loosely organized cellular architecture [2,8].

Numerous studies have sought to establish reliable MRI criteria for distinguishing benign from malignant tumors and for characterizing histological subtypes. The integration of advanced techniques, including DWI with apparent ADC measurement and DCE-MRI, has shown promise in improving diagnostic accuracy [3,6]. Challenges remain due to the variability in radiological presentations and the overlap in characteristics among certain tumor entities.

Our study aims to illustrate the main MRI characteristics of parotid tumors, focusing on signs that can help differentiate them, and to correlate multiparametric MRI features with histopathological findings to determine the most reliable diagnostic criteria for clinical practice.

## 2. Materials and Methods

### *Study design and population*

Our retrospective and analytical study was conducted within the ENT, Head and Neck Surgery Department of Farhat Hached University Hospital in Sousse. The study was conducted over 12 years from 2011 to 2023, including 42 patients with clinically suspected parotid tumors. As this was a retrospective study, we were reliant on existing medical records, which may have resulted in incomplete data for some variables. To minimize this limitation, only patients with complete preoperative MRI data and histopathological confirmation were included. The inclusion criteria were the presence of a clinically palpable parotid mass, the performance of a preoperative MRI, and histopathological confirmation of the diagnosis. Exclusion criteria were a history of prior parotid surgery, recurrent parotid tumors, inflammatory or infectious parotid lesions without histopathological confirmation of a neoplasm, incomplete MRI protocol, and missing radiological or histopathological data. Epidemiological, clinical, radiological, and histopathological data were collected from the patients' medical records.

### *MRI Protocol*

Standardized MRI protocols for evaluating parotid tumors included T1-weighted (T1W) and T2-weighted (T2W) sequences in axial, coronal, and sagittal planes. Fat suppression sequences (FAT SAT) were also used. Intravenous gadolinium was administered for post-contrast T1W sequences, allowing for the evaluation of tumor enhancement. In addition, diffusion-weighted imaging (DWI) sequences with ADC calculation and dynamic contrast-enhanced imaging (DCE-MRI) sequences were included in the protocol for further characterization of the lesions.

All MRI examinations were performed at the same institution (Sahloul University Hospital) using a consistent departmental protocol for parotid tumor evaluation. While minor adjustments to sequence parameters may have occurred over the study period, the core sequences (T1, T2, DWI with ADC, and DCE-MRI) and their diagnostic criteria remained stable. Image quality was assessed by experienced radiologists, and only examinations with adequate diagnostic quality were included.

For DCE-MRI, time-signal intensity curves were generated from regions of interest placed within the most enhancing solid portions of the tumor. Based on established criteria, these curves were classified into three types according to their morphology:

- **Type A (progressive enhancement):** gradual, continuous increase in signal intensity over time without a washout phase. This pattern is typically associated with paucicellular tumors such as pleomorphic adenoma.
- **Type B (rapid enhancement with washout):** fast initial upslope followed by a rapid decrease in signal intensity (washout). This pattern is characteristic of hypervascular tumors such as Warthin tumor.
- **Type C (rapid enhancement with plateau):** fast initial upslope followed by a plateau phase with no significant washout. This pattern is often observed in malignant tumors, including mucoepidermoid carcinoma 7,9.

### *Data Analysis*

MRI interpretation was performed by the Radiology Department at Sahloul University Hospital. The parameters evaluated included location (superficial lobe, deep lobe, or both), mass size, margin regularity (well-defined, irregular, infiltrative), presence of a capsule (visualized as a low signal on T1 and T2), homogeneity of signal on T1 and T2, and type and intensity of enhancement after gadolinium injection (homogeneous, heterogeneous, peripheral, weak, strong). ADC values were measured by placing regions of interest (ROIs) within the solid components of the tumors, avoiding cystic or necrotic areas. For DCE-MRI, time-signal intensity curves were classified into three types as previously described.

The MRI results were correlated with the histopathological results obtained after surgery. Statistical analysis using SPSS software was performed to assess the concordance between radiological and histological diagnoses. Agreement was assessed using the kappa coefficient, interpreted as follows: ≤0,20 poor, 0,21–0,40 fair, 0.41–0.60 moderate, 0.61–0.80 good, and 0.81–1.00 excellent agreement. The statistical significance of kappa values was tested against the null hypothesis of kappa = 0 (no agreement beyond chance), with p- value < 0.05 considered significant. In addition, 95% confidence intervals were calculated for all kappa estimates to provide a measure of precision.

Given the rarity of parotid tumors, the small sample size (n=42) and the low number of malignant tumors (n=5), non-parametric tests were preferentially used to avoid assumptions of normal distribution. Relevant MRI parameters were compared between benign and malignant tumors, as well as the various histological subtypes. The

Mann-Whitney U test was used for comparison between two groups, such as ADC values in benign versus malignant tumors, while the Kruskal-Wallis test was used for comparisons involving multiple histological subtypes. To reduce the risk of type I error associated with multiple comparisons, the Bonferroni correction was applied where appropriate. For example, when comparing ADC values across several histological subtypes, the significance threshold for pairwise comparisons was adjusted to $p < 0.016$ (0.05/3).

The small sample size, particularly for malignant lesions (n=5), is acknowledged as a limitation that may increase the risk of type II error. All statistical tests were two-tailed, and a p-value $< 0.05$ was considered statistically significant unless otherwise specified for multiple comparisons.

## 3.Results

*Epidemiological Data*

Our study included 42 patients suspected of having parotid tumors. The average age of patients was 44.6 years, with a male predominance of 61.9% (n=26) and a sex ratio of 1.6.

*Clinical examination*

The average size of the masses was 35 mm [10 to 80 mm]. Tenderness was noted in 7 patients (16.6%). The mass was found to be fixed in 4 patients (9.5%). In terms of consistency, the majority of tumors were firm (35 cases, 83.3%), while only one case (2.3%) was soft, and 4 cases (9.5%) were hard. Infiltration of the subcutaneous tissues was observed in 7 cases (16.6%). Peripheral facial paralysis was observed in 4 patients (9.5%). Cervical lymphadenopathy was present in 8 cases (19%).

*MRI results*

In our study, the location of the mass was predominantly unilateral, with 21 cases on the right side and 19 on the left side. In terms of anatomical distribution, 14 tumors were located in the superficial lobe, 12 in the deep and superficial lobe, and 2 in the deep lobe. The mean tumor size on MRI was 38 mm. A capsule, visualized as a low signal on T1 and T2, was observed in 19 cases (45.2%). Among these cases, there were 12 cases of pleomorphic adenomas (63.1%) (Figure 1), three cases of Warthin tumors (15.79%), one case of cystic lymphangioma (5.26%), one case of retention cyst (5.26%), one case of mucoepidermoid carcinoma (5.26%), and one case of acinic cell carcinoma (5.26%) (Figure 2).

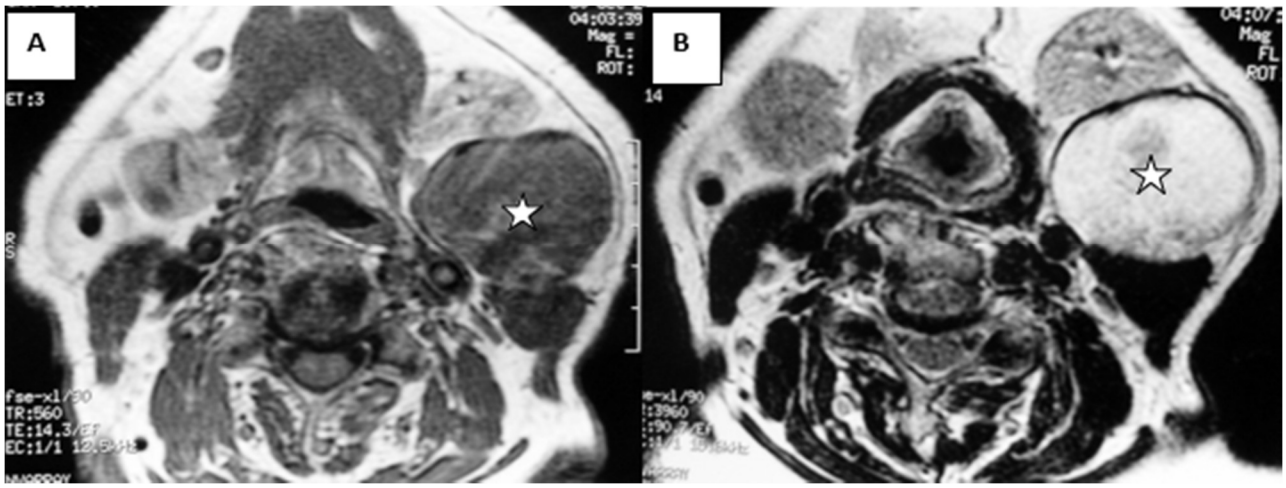


**Fig 1.** Axial T1 (A) and T2 (B) images: rounded encapsulated mass in the left parotid gland (star), (capsule with low signal intensity on T1 and T2), with heterogeneous signal intensity, hypointense on T1 and hyperintense on T2 (pleomorphic adenoma).

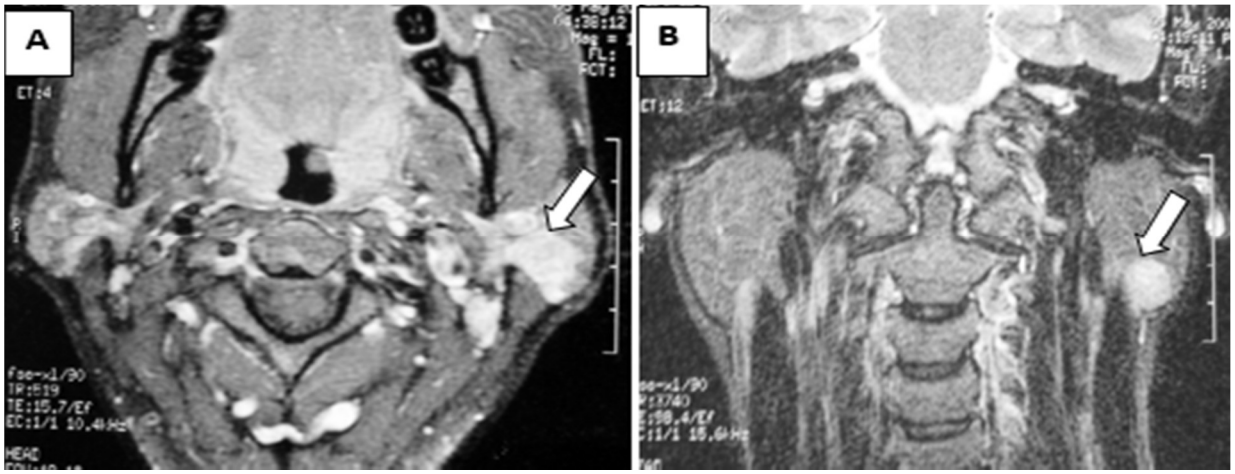


**Fig 2.** Axial T1 FAT SAT GADO (A) and coronal T2 FAT SAT (B) images: lesion of the lower pole of the left parotid gland (arrow), with irregular contours, T2 hypersignal, intensely and homogeneously enhanced by PDC (acinar cell carcinoma).

Hyperintensity on T2-weighted images was observed in 97.6% of cases, with 88% being malignant and 12% benign. Only one case (2.4%), a Warthin tumor, showed hypointensity on T2WI. Hyperintensity on T2WI correlated with tumor benignity. Nevertheless, T2WI hypointensity does not predict tumor benignity or malignancy. Regarding the signal on T1WI, 6 cases (14.2%) showed areas of hypersignal (5 Warthin tumors, 1 lipoma), with the remaining cases showing a hyposignal on T1WI. The signal was homogeneous in 7 cases (16.67%): 3 pleomorphic adenomas, 1 Warthin tumor, 1 lipoma, 1 retention cyst, and 1 lymphoepithelial cyst. It was heterogeneous in 34 cases, all of which were found to be malignant. After gadolinium administration, 93% of cases showed strong enhancement, including 2 cases of pleomorphic adenoma with peripheral enhancement (Figure 3). Only 7% of cases showed weak enhancement (1 lymphoepithelial cyst, 1 retention cyst, and 1 lipoma) (Figure 4).

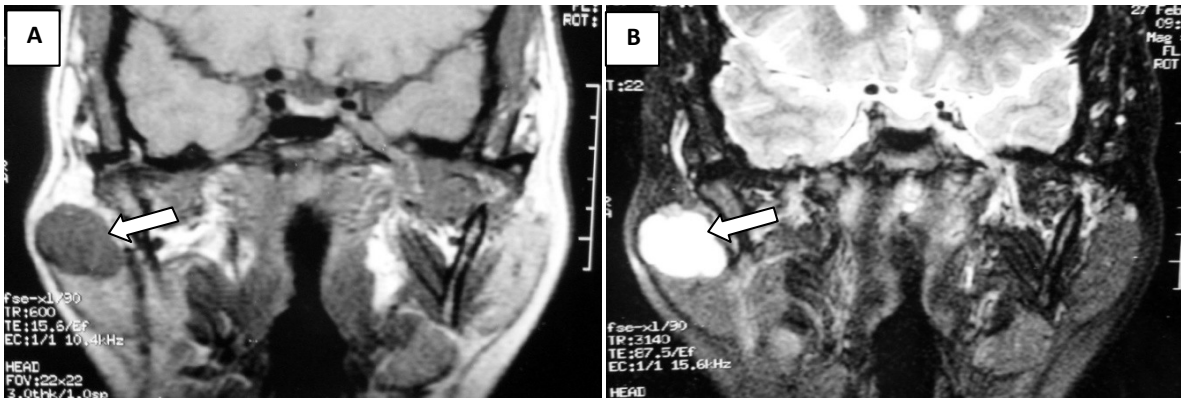


**Fig 3.** Coronal T1 WI (A) and T2 FAT SAT (B) images: well-defined mass (arrow) with polylobed contours in the superficial lobe of the right parotid gland, showing low signal intensity on T1 and clear, homogeneous high signal intensity on T2: pleomorphic adenoma.

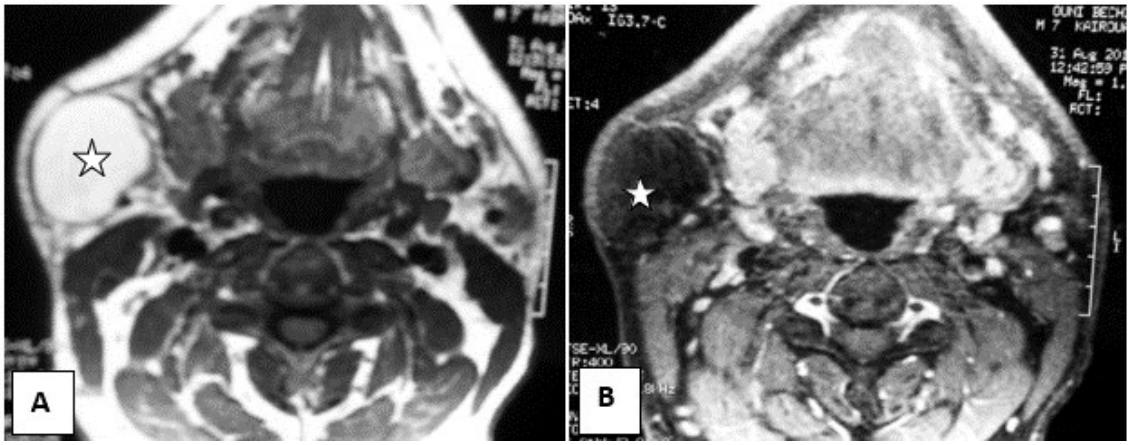


**Fig 4**. Axial T1 (A) and T1 FAT SAT GADO (B) images: encapsulated mass in the superficial lobe of the right parotid gland (star), with spontaneous homogeneous T1 hypersignal, suppressed on fat saturation sequences (parotid lipoma).

The ADC and DCE-MRI sequences were evaluated. For pleomorphic adenoma (Figure 5), we observed a bright signal on DWI with an ADC value of 1.56 and a type A enhancement curve. For Warthin tumor (Figure 6), a bright signal was observed on DWI with an ADC of 0.89 and a type B enhancement curve. For mucoepidermoid carcinoma (Figure 7), a bright DWI signal was observed with an ADC of 1.15 and a type C enhancement curve. ADC values of malignant tumors were significantly lower than those of benign tumors ($p < 0.05$).

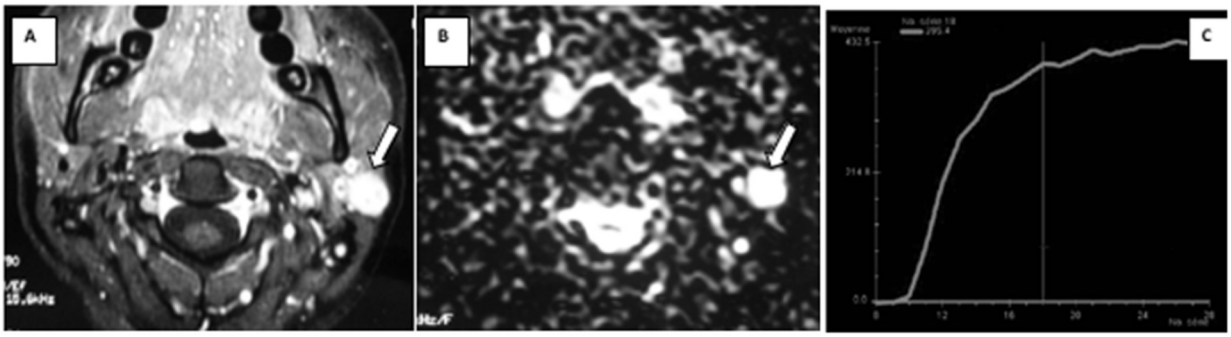


**Fig 5**. T1 FAT SAT GADO axial images (A) and diffusion (B): left parotid lesion (arrow) intensely enhanced by gadolinium, hypersignal on diffusion sequence (ADC = 1.56). The dynamic enhancement curve (C) is type A (pleomorphic adenoma).

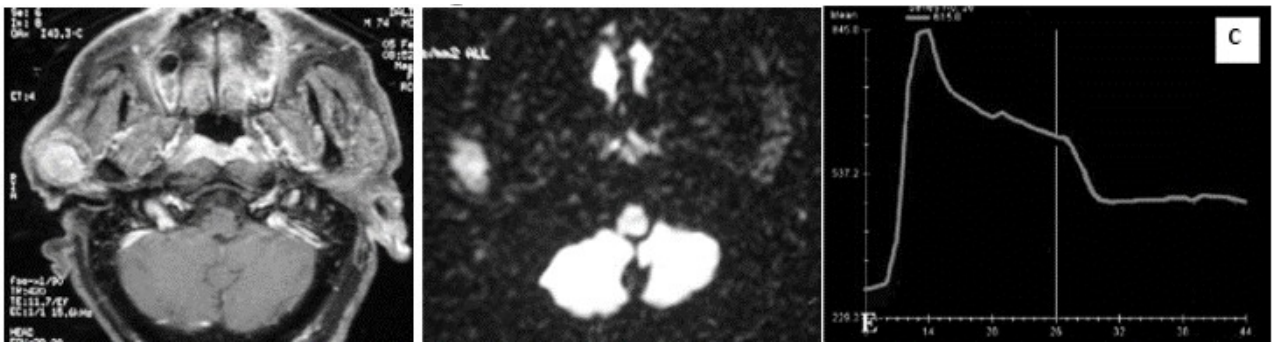


**Fig 6**. T1 FAT SAT GADO axial images (A) and diffusion (B): right parotid lesion (arrow), intensely and heterogeneously enhanced by gadolinium, with hypersignal on the diffusion sequence (ADC=0.89). The dynamic enhancement curve (C) is type B (Warthin tumor: cystadenolymphoma).

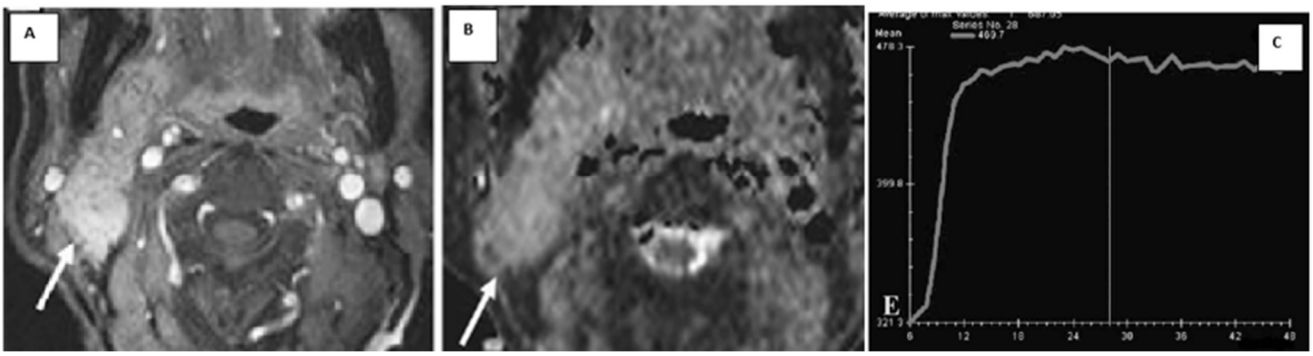


**Fig 7**: Axial T1 FAT SAT GADO (A) and diffusion (B) images: right parotid tumor (arrow), with irregular contours invading the parapharyngeal space, showing heterogeneous T2 hypersignal intensity, with intense and heterogeneous enhancement by gadolinium. ADC cartography of the tumor shows increased diffusion (ADC = 1.15). The dynamic enhancement curve (C) is type C (mucoepidermoid carcinoma).

Partial parotidectomy was performed in 24 cases, total parotidectomy in 10 cases, subtotal parotidectomy in 6 cases, and medical treatment in 2 cases.

The histological results of our study revealed a predominance of benign tumors (Table 1), accounting for 73.8% of cases (n=31), while malignant tumors (Table 2) accounted for 12% of cases (n=5). Pseudotumors accounted for 14.2% of cases (n=6).

The concordance between MRI findings and histological diagnoses was evaluated (Table 3). We found only moderate agreement between MRI and histological diagnosis for distinguishing benign from malignant tumors (kappa = 0.58; 95% CI: 0.41–0.75; $p < 0.005$).

However, significant concordance was observed between MRI findings and histological findings for the diagnosis of pleomorphic adenoma versus other tumors (kappa = 0.85; 95% CI: 0.72–0.94; $p < 0.005$). Similarly, concordance was significant for the diagnosis of Warthin tumors versus other tumors (kappa = 0.91; 95% CI: 0.80–0.98; $p < 0.005$).

**Table 1:** Histological distribution of benign parotid tumors.

| Histological type | Number of cases | Percentage (%) |
|---|---|---|
| **Benign tumors** | 31 | 73.8 |
| Pleomorphic Adenoma | 18 | 21.4 |
| Warthin Tumor | 9 | 4.2 |
| Lipoma | 1 | 2.3 |
| Hemangioma | 1 | 2.3 |
| Cystic Lymphangioma | 1 | 2.3 |
| Basal Cell Adenoma | 1 | 2.3 |

**Table 2:** Histological distribution of malignant parotid tumors.

| Histological type | Number of cases | Percentage (%) |
|---|---|---|
| **Malignant tumors** | 5 | 12 |
| Mucoepidermoid carcinoma | 1 | 2.3 |
| Acinic Cell Carcinoma | 1 | 2.3 |
| Cylindroma | 1 | 2.3 |
| Squamous Cell Carcinoma | 1 | 2.3 |
| Myoepithelial carcinoma | 1 | 2.3 |
| **Pseudotumors** | 6 | 14.2 |

**Table 3**: Concordance between MRI and histopathological findings.

| Diagnosis | Kappa value | Statistical significance |
|---|---|---|
| Benign tumors vs malignant | 0.58 ;95% CI: 0.41–0.75; p < 0.005 | Moderate agreement |
| Pleomorphic adenoma vs other tumors | 0.85 ; 95% CI: 0.72–0.94; p < 0.005 | Excellent agreement |
| Warthin tumor vs other tumors | 0.91 ; 95% CI: 0.80–0.98; p < 0.005 | Excellent agreement |

## 4. Discussion

Salivary gland tumors are rare, accounting for approximately 3% of all head and neck neoplasms, with the parotid gland being the most common site [8,10]. The risk of malignancy is inversely proportional to the size of the gland: tumors of the sublingual glands and minor salivary glands are more likely to be malignant, while those of the parotid gland are most often benign [10].

Parotid gland tumors exhibit a wide range of histopathological diversity, making their management complex [11,12]. According to the 2017 WHO classification of head and neck tumors, malignant tumors of the salivary glands are classified into 22 different types [7]. Clinical signs are often nonspecific. Some benign tumors may recur or become malignant, while some low-grade malignant tumors may clinically mimic benign lesions. Imaging, particularly MRI and CT, plays an essential role in locating the lesion, assessing its size, and guiding the therapeutic strategy [11]. MRI is the imaging modality of choice for evaluating salivary gland tumors [4]. However, due to their rarity and extreme histological/morphological diversity, it remains difficult for radiologists to establish a correct preoperative diagnosis of individual histological subtypes [7].

Our epidemiological data, with a mean age of 44.6 years and a sex ratio of 1.6, are compared with those in the literature, where variability in mean age and sex ratio is observed [6,12–14]. This variation could be attributed to geographical and demographic differences or to patient selection criteria (Table 4). The male predominance observed in our study is noteworthy, although the literature presents varied results in this regard.

**Table 4.** Comparison of epidemiological data with the literature.

| Authors | N | Mean age (years) | Sex ratio |
|---|---|---|---|
| Soylemez and Atalay (2021) | 42 | 51.4 | 0.75 |
| Elmokadem et al. (2019) | 52 | 51 | 1.36 |
| Zheng et al. (2018) | 45 | 62.3 | 1.5 |
| Tao et al. (2017) | 148 | 52 | 1.42 |
| Our study | 42 | 44.6 | 1.6 |

The cliniThe characteristics of the masses, such as average size and consistency, are consistent with the observations of Fassih et al., who found a firm mass in 54.6% of cases and a soft mass in 8% of cases [15].

Infiltration of subcutaneous tissue was observed in 7 cases (16.6%). Yuan et al. reported infiltration of adjacent tissue in 21.6% of malignant tumors compared to 1.9% of benign tumors, with a 15-fold increase in the risk of malignancy when adjacent structures were affected [16]. Facial nerve paralysis was observed in 9.5% of our patients. Inaka et al. reported facial paralysis in 18% of cases, exclusively in cases of malignant tumors [17]. Regarding cervical lymphadenopathy, our study showed an incidence of 19%, while Soylemez and Atalay found 11.1%. They emphasized that the presence of lymphadenopathy was significantly associated with malignant lesions [13]. These clinical signs, while suggestive of malignancy in some cases, lacked sufficient sensitivity and specificity to be used alone, reinforcing the need for advanced imaging.

MRI is recognized for its ability to precisely locate parotid tumors and assess their extent. Our results confirm this ability. The distinction between superficial and deep lobe tumors, as well as bilateral involvement, is a key element in guiding diagnosis and therapeutic management. Although deep lobe involvement is traditionally considered a sign of a malignant tumor, certain inflammatory conditions and benign tumors, such as Warthin tumor, can also affect the deep lobe [13,14].

As for tumor size, our study, as reported by Soyelemez and Atalay, found no significant correlation between size and benignity, suggesting that size alone is not a reliable discriminating criterion [13].

On the other hand, margin morphology proved to be more informative. Kim et al. emphasized that the presence of poorly defined and/or infiltrating margins versus well-defined margins on MRI images is very useful in differentiating a high-grade malignant tumor from a low-grade malignant tumor or a benign tumor [1]. A clear margin is generally suggestive of a benign tumor, but some malignant tumors can mimic this appearance [14]. Soylemez and Atalay reported that 22.2% of lesions had poorly defined margins and demonstrated that this morphological criterion was significantly associated with malignant tumors [13].

The detection of a capsule, often associated with pleomorphic adenomas, is another important criterion, as shown by our results and those reported in the literature [7,18].

In our study, a capsule was observed in 66.67% of pleomorphic adenoma cases, consistent with the literature, but was also present in one case of mucoepidermoid carcinoma and one case of acinic cell carcinoma, highlighting that this feature, while suggestive, is not pathognomonic.

Signal analysis and gadolinium enhancement also provided valuable information. Dynamic MRI with gadolinium injection can help differentiate benign from malignant tumors of the parotid gland [8,18]. Malignant tumors show more marked hypointense signals on T2-WI than benign tumors, while a hyperintense signal on T2-WI tends to indicate a benign lesion [5,14,19]. Our results

partially align with these observations; T2 hyperintensity was observed in 97.6% of cases, with 88% of these cases being benign. However, the single case of T2 hypointensity was a Warthin tumor, a benign entity, underscoring the overlap that limits the diagnostic utility of T2 signal alone.

Contrast enhancement, although strong in most cases, did not reliably distinguish benign from malignant tumors in our study, which was consistent with the findings of other studies in the literature [5,13]. However, the type of enhancement (homogeneous, heterogeneous, or peripheral) can point to certain diagnoses, such as the peripheral enhancement of pleomorphic adenomas.

The integration of DWI and DCE-MRI sequences represents a significant advance. Conventional MRI, even with injection, has limitations in differentiating benign parotid tumors from low-grade malignant tumors.

DWI MRI, by measuring the movement of water molecules, provides a more detailed assessment of tissue structure and activity, which can improve tumor characterization [8]. The low density of cellular components and increased interstitial space generate high diffusion with high ADC values (benign lesions) [2,20,21]. Our results, in agreement with Stoia et al., show that the ADC values of malignant tumors [0.91–1.2] are significantly lower than those of benign tumors [1.04–1.8] (except for pleomorphic adenoma [1.2–2.2] and Warthin tumor [0.72–1.2]) [2].

In addition, ADC measurements and characteristic dynamic enhancement patterns have shown value in suggesting specific histological subtypes. In particular, Type A curves are typically associated with pleomorphic adenoma, Type B curves with Warthin tumor, and Type C curves with mucoepidermoid carcinoma [3].

The single case of mucoepidermoid carcinoma in our study demonstrated a Type C curve, consistent with the pattern described for malignant tumors. However, given the small number of malignant cases, we cannot draw definitive conclusions about the reliability of this pattern for malignancy detection.

A meta-analysis by Li et al. confirmed significantly lower ADC values in malignant tumors but emphasized the need for standardized acquisition protocols and threshold values [11]. Similarly, Kato et al. highlighted the utility of combining ADC with DCE-MRI parameters to improve diagnostic accuracy [8].

These multiparametric techniques improve the ability of MRI to differentiate parotid tumors and predict their histological nature.

The therapeutic approaches to parotid tumors are mainly surgical, with variations depending on the benign or malignant nature of the lesion.

For example, in the case of a pleomorphic adenoma, surgery is generally indicated due to the significant risk of malignant transformation [4,7]. This risk is estimated at approximately 25% [4]. On the other hand, Warthin tumor, which rarely undergoes malignant transformation, does not always require surgical treatment. In this case, therapeutic abstention may be preferred to avoid the risk of facial nerve damage associated with the procedure 7. In our series, the excellent concordance for Warthin tumor (kappa = 0.91) suggests that MRI can reliably identify this entity, potentially sparing patients unnecessary surgery.

For malignant tumors, accurate preoperative characterization remains challenging. In our study, the moderate agreement (kappa = 0.58) for benign-malignant differentiation reflects this difficulty. However, MRI still provides crucial information for surgical planning in suspected malignancies, including depth of invasion, facial nerve involvement, and nodal status. This information directly influences the decision between partial and total parotidectomy and the need for neck dissection.

It is important to note that in our series, MRI served as a complementary tool to clinical assessment and FNAC, helping to refine the surgical approach and preoperative discussion with patients regarding expected outcomes and potential complications.

Despite the modest size of our study, excellent concordance was demonstrated between MRI findings and histopathological findings for specific diagnoses, particularly pleomorphic adenoma (kappa = 0.85) and Warthin tumor (kappa = 0.91), highlighting the diagnostic value of MRI for these entities. All patients in our study underwent a particularly complete MRI protocol, incorporating not only conventional sequences, but also diffusion techniques (DWI) with ADC calculation and dynamic gadolinium-enhanced MRI.

However, our study has several limitations. First, the relatively small size of our study (n=42), and particularly the low number of malignant tumors (n=5, 11.9%), limits the statistical power of our analysis. A study with a larger sample size and a more balanced distribution of histological types would be necessary to confirm our observations. Second, the retrospective nature of the study introduces potential selection and data collection biases. Despite strict inclusion criteria, we cannot exclude the possibility that some patients with incomplete data or atypical presentations were excluded. Third, the 12-year study period introduces potential technical variability due to MRI scanner upgrades, software updates, and minor protocol adjustments over time. While all examinations were performed at the same institution using a consistent departmental protocol, and image quality was verified by experienced radiologists, subtle differences in image acquisition may have influenced quantitative parameters such as ADC values or dynamic curve morphology. Fourth, interobserver variability was not systematically assessed in this study. Although MRI interpretation was performed by experienced radiologists, the lack of formal interobserver agreement analysis limits our understanding of the reproducibility of the reported findings. Finally, a critical aspect of diagnostic test evaluation is the false-positive and false-negative MRI interpretations. A capsule, typically found in pleomorphic adenoma, was observed in one case of mucoepidermoid carcinoma and one case of acinic cell carcinoma. Conversely, a Warthin tumor with atypical features, including heterogeneous signal and irregular margins, was initially misinterpreted as malignant, representing a false-positive case. The low ADC value of Warthin tumor overlaps with the malignant range, contributing to diagnostic uncertainty in some cases. These discordant cases highlight the limitations of MRI and underscore the continued need for histopathological confirmation. They also emphasize the importance of a multiparametric approach, as reliance on any single feature, whether a capsule, ADC value, or enhancement pattern, risks misdiagnosis.

Larger, prospective multicenter studies with standardized imaging protocols are needed to validate the diagnostic performance of multiparametric MRI for parotid

tumors. Such studies should aim to include sufficient numbers of malignant tumors to allow meaningful subgroup analysis and to establish reliable ADC thresholds for different histological types.

## 5. Conclusion

Despite these limitations, our results highlight the importance of multiparametric MRI in the preoperative diagnosis of parotid tumors. Multiparametric MRI provides excellent diagnostic accuracy for pleomorphic adenoma and Warthin tumor, aiding preoperative planning for these common benign entities. However, its overall performance in distinguishing benign from malignant parotid tumors is only moderate (kappa = 0.58), and the small number of malignant cases in our series limits conclusions about malignancy detection. Histopathological confirmation, therefore, remains essential, particularly when MRI features are atypical or suggest malignancy. Larger studies are needed to further define the role of MRI in the diagnostic algorithm for parotid tumors.

## Ethical Considerations

The study was conducted in accordance with the ethical standards of the institutional and national research committees and with the principles of the 1964 Declaration of Helsinki and its subsequent amendments.

## Consent for publication

All authors consented to the publication of the article.

## Declaration of Competing Interests

The authors declare that they have no conflicts of interest.

## Funding

This research did not receive any specific grant from funding agencies.

## Acknowledgment

None.

## References

[1] Kim SY, Borner U, Lee JH, Wagner F, Tshering Vogel DW. Magnetic resonance imaging of parotid gland tumors: a pictorial essay. BMC Med Imaging. 2022;22(1):191. https://doi:10.1186/s12880-022-00924-0

[2] Stoia S, Băciuț G, Lenghel M, et al. Cross-sectional imaging and cytologic investigations in the preoperative diagnosis of parotid gland tumors - An updated literature review. Bosn J Basic Med Sci. 2021;21(1):19-32. https://doi:10.17305/bjbms.2020.5028

[3] Coudert H, Mirafzal S, Dissard A, Boyer L, Montoriol PF. Multiparametric magnetic resonance imaging of parotid tumors: A systematic review. Diagn Interv Imaging. 2021;102(3):121-30. https://doi:10.1016/j.diii.2020.08.002

[4] Abdel Razek AAK, Ashmalla GA, Gaballa G, Nada N. Pilot study of ultrasound parotid imaging reporting and data system (PIRADS): Inter-observer agreement. Eur J Radiol. 2015;84(12):2533-8. https://doi:10.1016/j.ejrad.2015.09.001

[5] Gökçe E. Multiparametric Magnetic Resonance Imaging for the Diagnosis and Differential Diagnosis of Parotid Gland Tumors. J Magn Reson Imaging. 2020;52(1):11-32. https://doi:10.1002/jmri.27061

[6] Tao X, Yang G, Wang P, et al. The value of combining conventional, diffusion-weighted and dynamic contrast-enhanced MR imaging for the diagnosis of parotid gland tumours. Dentomaxillofacial Radiol. 2017;46(6):20160434. https://doi:10.1259/dmfr.20160434

[7] Takita H, Takeshita T, Shimono T, et al. Cystic lesions of the parotid gland: radiologic-pathologic correlation according to the latest World Health Organization 2017 Classification of Head and Neck Tumours. Jpn J Radiol. 2017;35(11):629-47. https://doi:10.1007/s11604-017-0678-z

[8] Kato H, Kawaguchi M, Ando T, et al. Current status of diffusion-weighted imaging in differentiating parotid tumors. Auris Nasus Larynx. 2023;50(2):187-95. https://doi:10.1016/j.anl.2022.07.002

[9] Espinoza S, Halimi P. Key elements in interpreting MRI scans of parotid tumors. Ann Fr Oto-Rhino-Laryngol Pathol Cervico-Faciale. 2013;130(1):30-6. https://doi:10.1016/j.aforl.2012.05.009

[10] Maraghelli D, Pietragalla M, Cordopatri C, et al. Magnetic resonance imaging of salivary gland tumours: Key findings for imaging characterisation. Eur J Radiol. 2021;139:109716. https://doi:10.1016/j.ejrad.2021.109716

[11] Li ZQ, Gao JN, Xu S, et al. Multimodal magnetic resonance imaging for the diagnosis of parotid gland malignancies: systematic review and meta-analysis. Transl Cancer Res. 2022;11(7). https://doi:10.21037/tcr-22-695

[12] Zheng N, Li R, Liu W, Shao S, Jiang S. The diagnostic value of combining conventional, diffusion-weighted imaging and dynamic contrast-enhanced MRI for salivary gland tumors. Br J Radiol. Published online June 27, 2018:20170707. https://doi:10.1259/bjr.20170707

[13] Orhan Soylemez UP, Atalay B. Differentiation of Benign and Malignant Parotid Gland Tumors with MRI and Diffusion Weighted Imaging. Medeni Med J. 2021;36(2):138-45. https://doi:10.5222/MMJ.2021.84666

[14] Elmokadem AH, Abdel Khalek AM, Abdel Wahab RM, et al. Diagnostic Accuracy of Multiparametric Magnetic Resonance Imaging for Differentiation between Parotid Neoplasms. Can Assoc Radiol J. 2019;70(3):264-72. https://doi:10.1016/j.carj.2018.10.010

[15] Fassih M, Abada R, Rouadi S, et al. Salivary gland tumors: epidemiological and clinical study and anatomo-radiological correlation: retrospective study of 148 cases. Pan Afr Med J. 2014;19. https://doi:10.11604/pamj.2014.19.187.820

[16] Yuan Y, Tang W, Tao X. Parotid gland lesions: separate and combined diagnostic value of conventional MRI, diffusion-weighted imaging and dynamic contrast-enhanced MRI. Br J Radiol. 2016;89:20150912.https://doi:10.1259/bjr.20150912

[17] Inaka Y, Kawata R, Haginomori S ichi, et al. Symptoms and signs of parotid tumors and their value for diagnosis and prognosis: a 20-year review at a single institution. Int J Clin Oncol. 2021;26(7):1170-8. https://doi:10.1007/s10147-021-01901-3

[18] Tartaglione T, Botto A, Sciandra M, et al. Differential diagnosis of parotid tumors: which MRI characteristics should be considered? Acta Otorhinolaryngol Ital. 2015;35(5):314-20. https://doi:10.14639/0392-100X-693

[19] Afzelius P, Nielsen M, Ewertsen C, Bloch KP. Imaging of the major salivary glands. Clin Physiol Funct Imaging. 2016;36(1):1-10. https://doi:10.1111/cpf.12199

[20] Munhoz L, Ramos EADA, Im DC, et al. Application of diffusion-weighted magnetic resonance imaging in the diagnosis of salivary gland diseases: a systematic review. Oral Surg Oral Med Oral Pathol Oral Radiol. 2019;128:280-310. https://doi:10.1016/j.oooo.2019.02.020

[21] Zhang W, Zuo Z, Huang X, Jin G, Su D. Value of Diffusion-Weighted Imaging Combined with Susceptibility-Weighted Imaging in Differentiating Benign from Malignant Parotid Gland Lesions. Med Sci Monit Int Med J Exp Clin Res. 2018;24:4610-6. https://doi:10.12659/MSM.911185

Cite this article as: El Omri M, Dakhli I, Bellakhdher M, Thabet N, Kermani W. The role of multiparametric magnetic resonance imaging (MRI) (DWI and DCE-MRI) in differentiating parotid tumors: A retrospective study of 42 cases. Biomedicine Healthcare Res. 2026;7:42-50. https://doi.org/10.71599/bhr.v7i1.182